UCRL- 85645
PREPRINT

CONF-810910--26

ABERRATIONS AND FOCUSABILITY IN LARGE SOLID-STATE-LASER SYSTEMS

W. W. Simmons

THIS PAPER WAS PREPARED FOR SUBMITTAL TO
Society of Photo-Optical Instrumentation
Engineers International Symposium &
Instrument Display
(SPIE)

San Diego, California - August 24-28, 1981

August 26, 1981

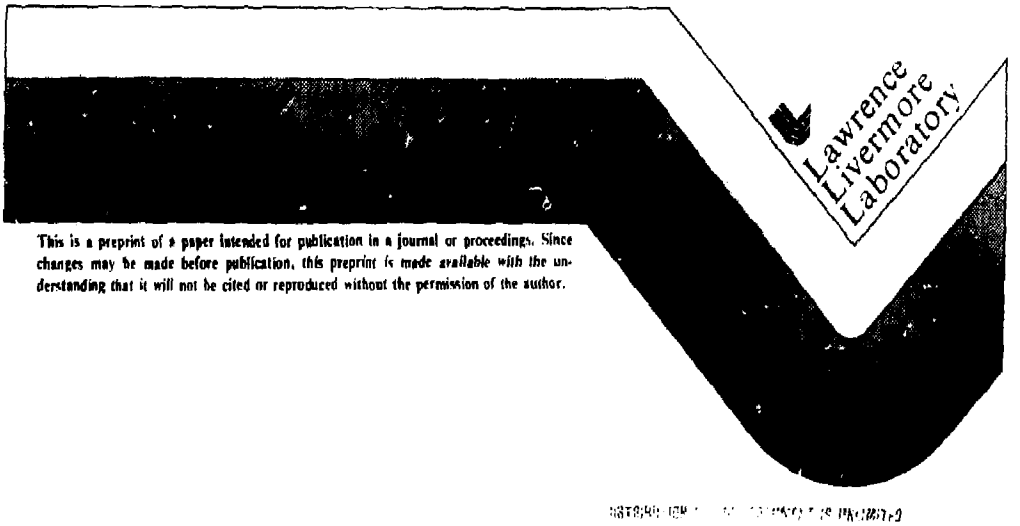

ABERRATIONS AND FOCUSABILITY IN LARGE SOLID-STATE-LASER SYSTEMS*

W. W. Simmons

University of California, Lawrence Livermore National Laboratory
P. O. Box 5508, Livermore, California 94550

Abstract

Solid state lasers for fusion experiments must reliably deliver maximum power to small (approximately .5 mm) targets from stand-off focal distances of 1 m or more. This requirement places stringent limits upon the optical quality of the several major components -- amplifiers, Faraday isolators, spatial filters -- in each amplifier train. Residual static aberrations in optical components are transferred to the beam as it traverses the optical amplifier chain. Although individual components are typically less than $\lambda/20$ for components less than 10 cm clear aperture; and less than $\lambda/10$ for components less than 20 cm clear aperture; the large number of such components in optical series results in a wavefront error that may exceed one wave for modern solid state lasers. For pulse operation, the focal spot is additionally broadened by intensity dependent nonlinearities. Specific examples of the performance of large aperture components will be pre- sented within the context of the Argus and Shiva laser systems, which are presently operational at Lawrence Livermore National Laboratory. Design requirements upon the larger aperture Nova laser components, up to 74 cm in clear aperture, will also be discussed; these pose a significant challenge to the optical industry.

---

*Research performed under the auspices of the U. S. Department of Energy by the Lawrence Livermore National Laboratory under contract number W-7405-ENG-48.

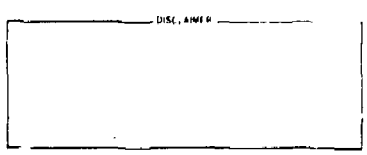

Introduction

The focusability of high energy pulses from large laser systems is determined in part by the quality of the optical components through which the beam passes, and in part by nonlinear, intensity dependent phase retardation, which is in turn proportional to the material refractive properties of these components. In this article, we shall discuss these sources of focal spot broadening, with particular emphasis on high power solid state lasers. Representative data were taken with the Shiva laser[1] at Lawrence Livermore National Laboratory. This system will be used in this article as an example of modern solid state laser design and performance. Component specifications for the much larger Nova laser system,[2] presently under construction at LLNL, will be presented for comparison.

Solid state lasers are designed in a master-oscillator pulsed amplifier (MOPA) configuration. A weak pulse (about 1 mJ in 1 ns) is generated by an optical oscillator and electrooptic switch. This pulse is subsequently shaped (both spatially and temporally), amplified, and split into several beams (20 for Shiva and Nova). Each of the several beams then propagates through components of successively larger clear aperture, culminating in a refractive lens system that focuses each beam onto a small ($\leq$1 mm) target.

The components comprising each laser amplifier chain perform three major functions:

(1) Rod and disk amplifiers increase the power and energy of the pulse.

(2) Spatial filters maintain the smoothness of the beam profile while expanding its diameter.

(3) Pockels and Faraday isolators prevent the entire laser from breaking spontaneously into oscillations that could drain its stored energy and damage the target prematurely.

Conceptually, amplification, spatial filtering and isolation are repeated sequentially, at ever-increasing apertures, as the pulse proceeds down the chain. Ultimately, each pulse is focused with a lens.

In this article, we shall examine several causes of spreading of the final focal spot. These may be categorized as follows:

(1) Static aberrations transferred to an otherwise diffraction limited beam by the optical components through which it passes.

(2) Small-angle scattering by small damage sites, inclusions, inhomogeneity, etc.

(3) Nonlinear enhancement of spatial modulation on the transverse beam wavefront.

Static Aberrations

Residual aberrations in all optical components are transferred to the beam as it traverses the optical amplifier chain. Although individual components are held to very tight tolerances in manufacturing, the large number of such components in (optical) series can result in a significant wavefront error at the output of the chain.

There are six basic optical materials in the laser amplifier train:

- o BK-7 (lenses, mirrors, polarizers)
- o KD*P (Pockels' cell isolators)
- o Crystal Quartz (waveplates)
- o Nd-doped silicate (or phosphate) rod and disk amplifiers
- o Tb:doped silicate glass (Faraday rotators)
- o Fused Silica (some lenses)

Most of these components have flat optical surfaces. However, there are several f/1 lenses, which are in general aspherized to eliminate spherical aberration (it is noteworthy that spatial filter lens designs can combine minimal coma with elimination of spherical aberration).

Components that transmit the beam are designed to be as thin as practical to reduce the effects of the nonlinear index of refraction of the laser-disk glass. For most flatwork, Shiva vendors made very effective use of modern continuous-polishing equipment, usually incorporating precise thermal control. For aspheric lens surfaces, vendors developed efficient techniques for figuring and process testing. Surfaces were generally ground and polished spherical before figuring.

The tolerance levels of the larger Shiva components are illustrated in the specifications in Table I. These specifications are as tight as feasible, considering budgetary and schedule constraints and the state-of-the-art. Performance characteristics and final specifications were often the result of extensive technical interaction between LLNL and participating vendors. They involved prototype development and extensive qualification tests.

A final test was performed on all Shiva optical components. Each subassembly (e.g., laser head, spatial filter, mounted mirror) was tested for wavefront distortion (and, where appropriate, stress birefringence) before installation in the laser. For this purpose, two 30 cm aperture interferometers were made available in one of the LLNL laser-assembly areas: a ~0.633 μm Fizeau with a special long bead; and a 1.06 μm, LLNL built Twyman-Green (residing on a 25 ton granite slab). To indicate the as-assembled quality of such components, Figure 1 shows typical wavefront interferograms for a six-disk, 9 cm aperture disk amplifier, a 21 cm aperture final focusing lens, and a 22 cm aperture polarizer substrate. All of these interferograms were taken double-pass at .633 μm with the Fizeau interferometer.

The disk amplifier wavefront distortion averages 0.10 λ at 1.06 μm, and is typical of 60 such amplifier assemblies used in Shiva. The lens is a single-element, f/6 refractor, fabricated from BK-7 glass, shaped for minimum coma and corrected for spherical aberration by aspherizing the front (more curved) surface. Both surfaces are hard-dielectric-coated for minimum reflection loss. The polarizer substrate, part of the 41 cm Faraday isolator assembly, is only 10 mm in thickness. It is mounted at Brewster's angle (56.4 degrees) with respect to the beam line. The inner surface inscribed on this interferogram represents the central zone, over which the slope error tolerance is specified more rigorously.

Spatial filters for Shiva were assembled and pumped down, then aligned as a unit using the Twyman-Green interferometer mentioned above, before

being mounted on the spaceframe. Axial separation between lenses was set during this alignment for collimated input and output beams, and was not adjusted thereafter.

The chart shown in Table 2 presents the optical components traversed by each Shiva beam. The pulse leaving the oscillator/switchout has a uniphase, slightly elliptical, Gaussian spatial profile. (Elliptical because of the characteristic tilting of the YAG laser rod at Brewster's angle within the optical cavity.) Small aperture components traversed by the Gaussian beam, prior to its entering the major components of each laser chain, include 3 rod amplifiers, 1 Faraday rotator, 13 lenses, 2 quartz waveplates, and about 27 mirrors/splitters/polarizers. Typical peak-to-valley wavefront errors are listed at the top of Table 2. The cumulative wavefront error of the beam at this point, assuming that component errors are uncorrelated, and that the beam from the oscillator/switchout is diffraction limited, is .38 waves, as shown in Table 2.

The beam forming aperture truncates the Gaussian beam at a radius much smaller than its transverse full-width half maximum dimensions. Thus the main amplifier chain components amplify and expand a reasonably flat-profiled, round beam which approximately fills available amplifier apertures. Specified aberrations for the components comprising each Shiva chain are shown in Table 2. It is seen that each main beam-line contributes about one-half wave to the total accumulated wavefront error; which, for Shiva, is about 0.6 waves.

In operational practice, additional effects also contribute to focal spot broadening. First, slight misalignments from stage to stage will offset the beam slightly on spatial filter lenses, thus contributing small amounts of both astigmatism and coma to the output beam wavefront. Second, errors in collimation of the beam contribute to astigmatism (a diverging or converging beam traversing tilted elements causes astigmatism). Finally, the output beam from the oscillator/switchout departs from diffraction-limited performance by a fraction of a wave. (Thermal lensing is, of course, compensated by imaging lenses, but residual aberrations are not.)

We have observed the effects of turbulence in the atmosphere through which the beam passes. However, we have found that enclosing the beam lines in sealed tubes, maintained at constant temperature (variations of $\pm$ 1^{0}C, by the excellent air flow system of the building, effectively eliminates turbulent focal spot blurring for Shiva. This approach will also be used on Nova.

Considering estimates of all of these static effects together, one arrives at the qualitative conclusion that a typical low-power Shiva beam should be focusable to about one wave. Figure 2 illustrates photographed beam characteristics for a low power (200 GW) pulse near the focus of the f/6 target lens. (These photographs were taken in planes equivalent to those shown in the sketch using an array camera[3] with lateral magnification of 12X.. One can distinguish both astigmatism and spherical aberration as the predominate Seidel aberrations, though the wavefront is obviously distorted in a more complex way. These beam

photos correspond well with CW alignment beam observations at equivalent locations. Ninety percent of the beam energy is delivered within a circle of 75 μm radius in the plane of best focus; and eighty percent appears within a circle of radius 50 μm.

The time-integrated, or energy density, analysis is shown more clearly in Figure 3, which illustrates the central photograph in Figure 2, analyzed and renormalized to plot beam brightness versus half-anglular beam divergence. It is observed that Shiva, like Argus[4] and other [illegible] operates at typically 10^{18} W/cm^2-ster. The curve is obtained by microdensitometer analysis of the photograph, and plots radially averaged intensity as a function of half-angle from the [illegible].

We have estimated the wavefront error on this 'typical' Shiva low [illegible] by adding third-order aberrations to the 'otherwise perfect' [illegible]. Figure 4 shows a reasonable approximation to the [illegible] obtained. Closer fits can obviously be obtained with a more detailed analysis. Nevertheless, the orders-of-magnitude [illegible]. The angular radius of the second Airy ring [illegible] of the far-field energy of a flat-profile beam, [illegible] diffraction-limited beam. In contrast, the experimental [illegible] 40% at [illegible] μrad (3.5 times diffraction-limited). The computation illustrates that this representative Shiva beam carries somewhat more than one wave of observations.

In Table 3, we show the Nova optical component specifications. These larger laser components might be compared with Shiva (see Table 1). Note that the total number of components is only increased by about 30% (134 vs 109). Also, again assuming that there is no correlation of wavefront error between individual components, the total accumulated error for the Nova beamline is expected to be only slightly larger than that for Shiva (.76λ vs .6λ), even though the final component apertures are almost four times as large. To achieve these component figuring accuracies is a demanding task for the United States optical industry. To illustrate the magnitude of the Nova system, Figure 5 shows mirror blanks to accommodate the 74 cm output beams from Nova. Approximately ninety such mirrors will be used in the full 20 beam Nova system.

Dynamic Aberrations; Distortion from Nonlinearities

In addition to the classical, static aberrations just discussed, high power laser beams are also significantly affected by an intensity-dependent phase distortion. The source of this distortion is the nonlinearity in the index of refraction in all of the transparent optical components through which the beam passes. The nonlinearity depends on both the temporal and transverse spatial properties of the beam intensity. The magnitude of the phase distortion (actually, a retardation) in radians is given by the equation

$$B(x,y) = k \int_0^L \alpha I(x,y)dz,$$

where k is the wave number of the laser radiation, α is the nonlinear index of refraction coefficient (in cm^2/watt), $I(x,y)$ is the beam intensity (in W/cm^2) at transverse coordinates x and y, and the integration path L includes all optical material along the central beam

ray. This nonlinearity has been the subject of many investigations,[5] since it is responsible for instabilities leading to beam self-focusing and a host of other performance-limiting effects. For present purposes, we are interested in low-spatial-frequency effects. The whole beam distortion arising from this phase retardation has been analyzed in some detail by Hunt, Renard and Nelson[6] for smooth intensity profiles. In the following paragraphs, the effects of radial "ripple" caused by low-pass spatial filtering will be discussed qualitatively.

For typical spatially filtered laser systems such as Shiva, the confocal lens pairs that comprise each filter also serve to "project" the spatial beam profile downstream. This image relaying[7] helps to maintain a smooth beam profile and a high amplifier aperture filling factor. In addition, the bending of light rays due to the nonlinear refractive index is very small. Consequently, the intensity profile of the beam does not change throughout the chain, while the phase distortion takes on a spatial character identical to the intensity profile.

The effects of scattering from small damage sites, dust particles, etc., are mostly manifest as near-field beam modulation. Since these sources produce a wide angular distribution in the far-field, they may be low-pass filtered periodically throughout the laser chain. This filtering is accomplished with "pinholes" located at the common focus of each spatial filter lens pair. Low-pass filtering, in turn, superposes a sinusoidal radial modulation upon the main beam (Gibbs phenomenon). The first spatial filter following the beam forming aperture essentially

defines the intensity profile of the beam. The pinhole diameter is chosen such that the radial "ripple" modulation depth (which increases with decreasing diameter) just balances the modulation depth from other upstream sources[7] at the output of the first filter. Typically, the acceptance angle of the filter is about a factor of ten larger than the diffraction limit. The resulting ripple modulation depth is then a few percent of the background beam.

As the beam proceeds along the amplifier chain, phase retardation of the intensity peaks (relative to valleys) accumulates. This accumulation is not generally significant in the near field, but can have dramatic consequences near the final focus of the target lens. As an example, Figure 6 shows calculated radial intensity profiles 6 mm upstream (and downstream) from the focus of an f/6 lens, for various laser beam intensities. At very low intensity (top), the beam is an excellent geometrical projection of the beam entering the lens. At intermediate intensities ($\simeq$.5 TW, B $\simeq$3 for Shiva), the outer edge of the beam has moved inward to form a "ring". At the highest intensity (1.5 TW, B $\simeq$9 for Shiva), the beam has noticeably collapsed inward, and several high-contrast rings are apparent. Beyond the focus, modulation depth variations are not as pronounced; nevertheless, beam spreading that increases with B is quite apparent.

In practice, of course, the radial symmetry of the "ripple" rings is perturbed by diffraction from small scattering sites localized at components within the laser chain. Beam photographs taken at high power in planes equivalent to these show clearly both the deep ring modulation and the symmetry break-up caused by small-site diffractive interference.

To summarize; phase retardation is proportional to I, and is manifest as a broadening of the focal spot, as well as a complicated distortion of the beam near the focal plane. In Figure 7, we show calculated, and measured, radial-average far field cumulative intensities versus angle for a high-power (1 TW) Shiva shot. The curve labelled "no aberrations" represents a diffraction limited beam, except that small scattering sites have been introduced along the chain, at locations corresponding to amplifier disk positions. The resulting "flare" (energy distributed from about 20 μrad outward) represents low-angle scattering from these small obscuring sites. (By low-angle, we mean that energy which the spatial filter pinholes will pass; typically, this is 200-300 μrad.) The obscuration density used in the calculation was equivalent to a fractional obscured area of 5×10^{-5} per surface, a number in agreement with detailed statistical analysis of Shiva disks[8] before and after operational use. (This number is also used to specify maximum density and size of small inclusions and bubbles within manufactured optical components; see, for example, Table 1. Similar quality specifications are used for Nova components.)

When astigmatism and spherical aberrations are also included, one obtains the intermediate curve (in Figure 7). Finally, by taking account of the radial "ripple" effects discussed above, one obtains reasonable agreement with the observed focal spot distribution (shown as the broadest distribution curve in Figure 7).

Summary

We have discussed various aspects of the focusing characteristics of high-power beams from solid-state laser systems. It has been shown that static component wavefront errors, small scattering sites, and low-pass "ripple" all combine to broaden the focal spot from such lasers. The refractive index nonlinearity broadens the focal plane distribution aditionally when the laser chain is operated at high power. Nevertheless, assuming that state-of-the-art component manufacturing/finishing methods are employed, such beams are readily focusable onto submillimeter laser fusion targets. These conclusions apply as well to Nova.

Acknowledgments

The author is indebted to E. P. Wallerstein for sharing his extensive expertise concerning the optical quality of the large laser components described here. He appreciates conversations with D. R. Speck and R. G. Ozarski, who collaborated to obtain and analyze the Shiva focal spot data. W. E. Warren performed the computational analyses given above with the two-dimensional computer code Malaprop.[9]

References

1. J. A. Glaze and R. O. Godwin, "Shiva: Its Components and Subsystems," Laser Focus, August, 1977.

2. J. F. Holzrichter, R. O. Godwin, W. F. Hagen, W. W. Simmons and J. B. Trenholme, "Nova System at Lawrence Livermore National Laboratory", Laser Focus, May, 1981.

3. I. M. Winer, "A Self-Calibrating Technique for Measuring Laser Beam Intensity Distributions," Appl. Optics 5, p. 1437 (1966).

4. W. W. Simmons, D. R. Speck and J. T. Hunt, "Argus Laser System: Performance Summary," Applied Optics 17, p. 999 (1978).

5. E. S. Bliss, J. T. Hunt, P. A. Renard, G. E. Sommargren and H. J. Weaver, "Effects of Nonlinear Propagation on Laser Focusing Properties," IEEE J. Quant. Elec. QE-12, p. 402 (1976).

6. J. T. Hunt, P. A. Renard and R. G. Nelson, "Focusing Properties of an Aberrated Laser Beam," Applied Optics 15, p. 1458 (1976).

7. J. T. Hunt, J. A. Glaze, W. W. Simmons and P.A. Renard, "Suppression of Self-Focusing through Low-Pass Spatial Filtering and Relay Imaging," Applied Optics 17, p. 2053 (1978).

8. I. F. Stowers and H. G. Patton, "Damage History of Argus," Ninth Symposium on Materials for High Power Lasers, Boulder, Colo., October 4-6, 1977. Published in NBS Special Pubication 509, p. 440 (1977).

9. W. W. Simmons, J. T. Hunt and W. E. Warren, "Light Propagation through Large Laser Systems," to be published in IEEE J. Quant. Elec., September, 1981.

Figure Captions

Figure 1. Interferograms of representative Shiva components. Left: 6-disk, 9 cm aperture disk amplifier. Center: f/6 focusing lens, designed for minimal coma and aspherized. Right: polarizer substrate.

Figure 2. Beam photographs taken in several planes near the plane of best focus of the Shiva f/6 focusing lens. The beam power is 200 GW at a pulse duration of 800 ps, for 160 joules of on-target energy.

Figure 3. Photograph and radially averaged densitometer scan of the beam in Figure 2, in the plane of best focus. Graph presents beam data in terms of brightness versus angular radius.

Figure 4. Calculated and measured cumulative radial-average far-field intensity for the beam shown in Figures 2 and 3. Malaprop computer code used for computation/simulation.

Figure 5. Mirrors made from these 1.2 m diameter glass blanks, made of borosilicate glass by Schott Optical Company, will be used to direct Nova beams to the target chamber.

Figure 6. Calculated beam profiles in planes $\pm$ 6 mm from the plane of best focus for an f/6 laser system. As intensity and B increase, these profiles become progressively more distorted, and also exhibit greater modulation depth.

Figure 7. Calculated and measured cumulative, radial average, far-field intensity for a high power (1 TW) Shiva shot, corresponding to a beam retardation B $\simeq$ 7-8, (with reference to Figure 6).

Table I. Tolerance Chart for Larger Components

Aperture Size	10 cm Spatial Filter			20 cm Spatial Filter		
	Disks	Lenses	Polarizers	Disks	Lenses	Polarizers
Inclusions/100 cm^3	0.03 mm^2 0.125 max dimension	0.03 mm^2 0.100 max dimension	0.03 mm^2 0.100 max dimension	0.03 mm^2 0.2 max dimension	0.03 mm^2 0.2 max dimension	0.03 mm^2 0.2 max dimension
Stress birefringence nm/cm	5	6.0	2.0	5.0	6.0	6.0
Wavefront P.V. - 0.633 μm after coating when applicable	$\lambda/12$	$\lambda/10$	$\lambda/12$	$\lambda/8$	$\lambda/10$	$\lambda/8$
Wavefront slope/cm (0.633 μm)	$\lambda/30$	$\lambda/33$ to $\lambda/22$	$\lambda/30$	$\lambda/40$ to $\lambda/22$	$\lambda/33$ to $\lambda/22$	$\lambda/30$ to $\lambda/20$

Table 2. Typical Shiva Beam Line Optical Components

Component	# of Optical Elements/Arm	Nominal Beam Diameter (mm)	Typical Peak-to Valley Wavefront Error per Assembly	Cumulative* Wavefront Error
Mirrors/Splitters	20	21*	λ/20	
Rod Amps	3	21*	λ/10	
Polarizers	7	21*	λ/20	
Faraday Rotator	1	21*	λ/10	
Lenses	13	21*	λ/20	
Waveplates	2	21*	λ/20	.38λ
Beam Forming Aperture	1	10	-	
Front-end Relay	2	21	λ/12	
Rod Amplifier	1	21	λ/10	
Polarizer	2	21		
Pockels Cell Assembly	3	21	λ/8	
Polarizer	2	21		
Spatial Filter	2	44	λ/12	
Rod Amplifier	1	44	λ/10	
Polarizer	2	44		
Pockels Cell Assembly	3	44	λ/7	
Polarizer	2	44		
Spatial Filter	2	91	λ/12	
Disk Amplifier	6	91	λ/10	
Disk Amplifier	6	91	λ/10	
Polarizer	2	91		
Faraday Rotator	1	91	λ/9	
Polarizer	2	91		
Spatial Filter	2	91	λ/12	
Disk Amplifier	6	91	λ/10	
Spatial Filter	2	145	λ/12	
Disk Amplifier	4	145	λ/10	
Spatial Filter	2	202	λ/12	
Polarizer	1	202		
Faraday Rotator	1	202	λ/9	
Polarizer	1	202		
Disk Amplifier	3	202	λ/8	
First Turn Mirror	1	202	λ/14	
Second Turn Mirror	1	202	λ/15	
Focus Lens	1	202		
Vacuum Window	1	185	λ/7	
Blast Shield	1	185		.48λ
	109 elements traversed by one element		Total accumulated wavefront error	.61λ

*FWHM of Gaussian beam profile

+Square root of sum of squares of individual component errors

Table 3. Nova Beam Line Optical Component Specifications

Component	# of Elements per Arm	Nominal Beam Diameter (mm)	Specified P-V Wavefront Error per Assembly	Cumulative Wavefront Error
Front-end Optics	50	27*	(.05-.1) λ typ.	
Beam-forming Aperture	1	27	-	.4λ
Spatial Filter	2	37.5	.09λ	
Rod Amp	1	37.5	.10λ	
Polarizers	2	37.5		
Pockels Cell Assy.	3	37.5	.08λ	
Polarizers	2	37.5		
Spatial Filter	2	91.7	.09λ	
Disk Amplifier	6	91.7	.12λ	
Polarizers	2	91.7		
Faraday Rotator	1	91.7	.13λ	
Polarizers	2	91.7		
Disk Amplifier	6	91.7	.12λ	
Spatial Filter	2	150	.09λ	
Faraday Rotator	1	150		
Polarizer Pair	2	150	.10λ	
Disk Amplifier	4	150	.12λ	
Spatial Filter	2	208	.09λ	
Polarizers	2	208		
Faraday Rotator	1	208	.16λ	
Polarizers	2	208		
Disk Amplifiers	9	208	.23λ	
Spatial Filter	2	315	.09λ	
Turning Mirrors	2	315	.10λ	
Polarizer	1	315		
Faraday Rotator	1	315	.13λ	
Polarizer	1	315		
Disk Amplifiers	8	315	.29λ	
Spatial Filter	2	460	.09λ	
Disk Amplifiers	6	460	.25λ	
Spatial Filter	2	740	.09λ	
Mirrors	4	740	.14λ	
Focusing Lenses	2	740	.09λ	.65λ
	84 Total Components per Chain		Total Accumulated Wavefront Error	.76λ

134 Total Components Traversed by Beam

*FWHM Gaussian Beam Profile

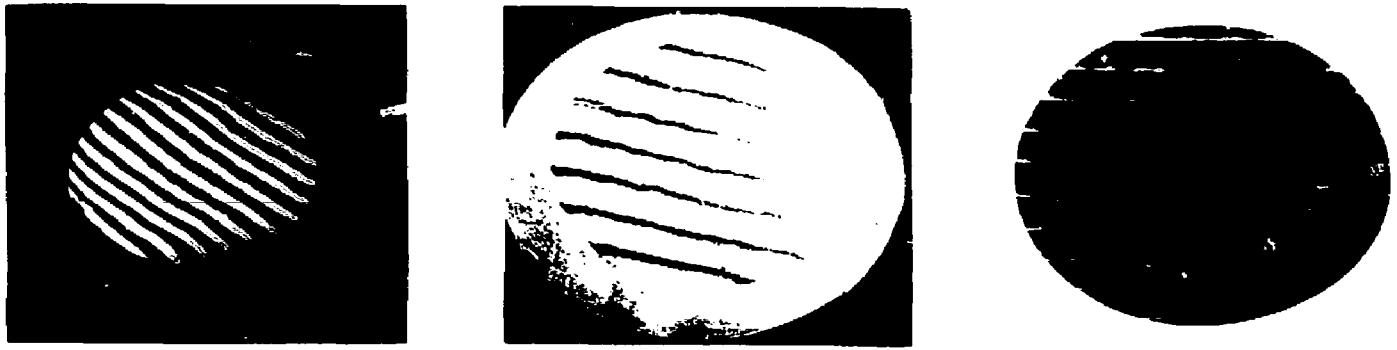

Figure 1

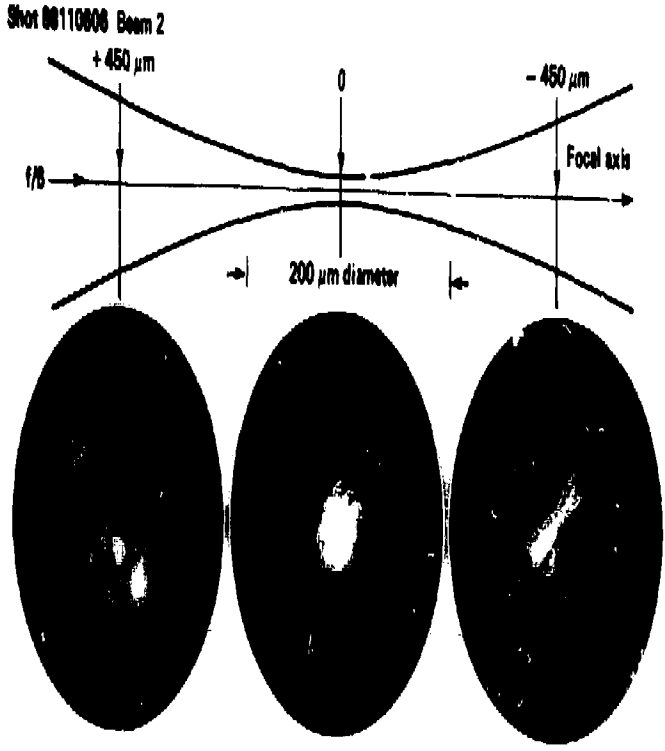
Shot 88110808 Beam 2
+ 450 µm
0
- 450 µm
f/8
Focal axis
200 µm diameter

Figure 2

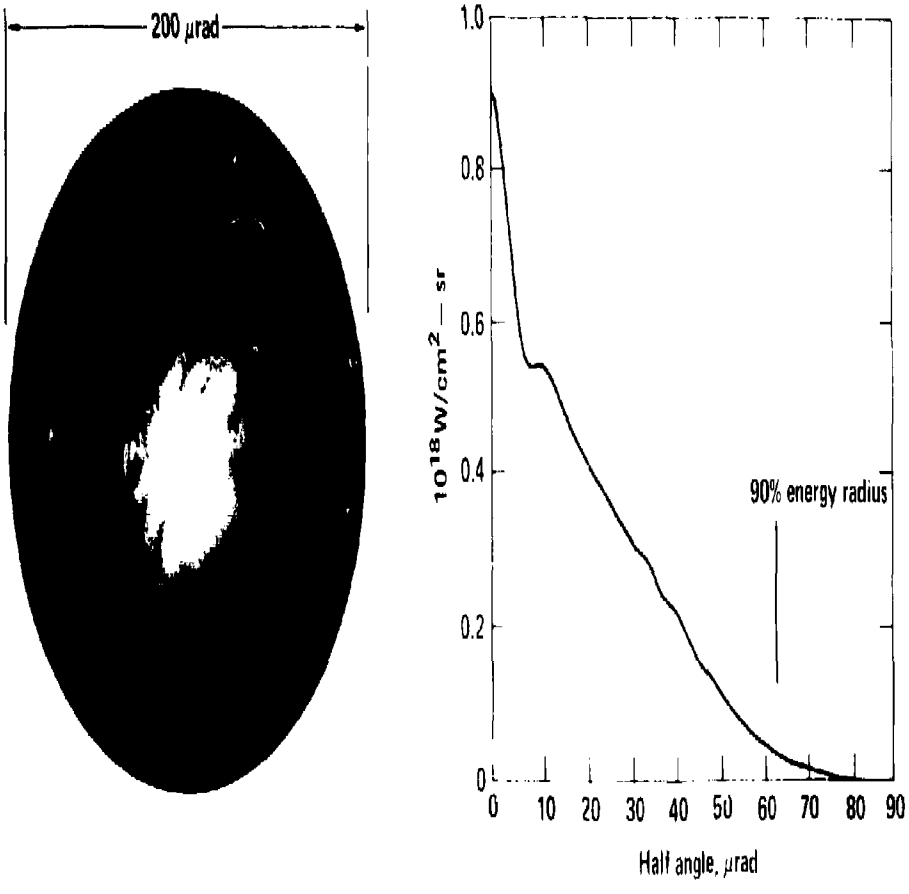
200 μrad
1.0
0.8
0.6
0.4
0.2
0
10^{18} W/cm^2 — sr
90% energy radius
0
10
20
30
40
50
60
70
80
90
Half angle, μrad

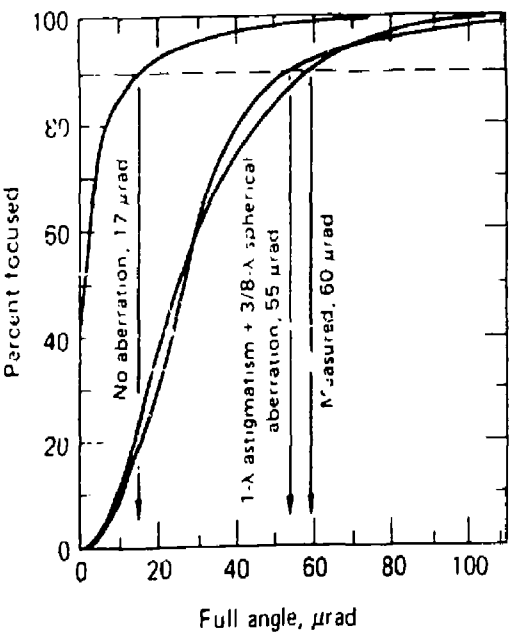
100
80
60
40
20
0
Percent focused
0
20
40
60
80
100
Full angle, μrad
No aberration, 17 μrad
1-λ astigmatism + 3/8-λ spherical aberration, 55 μrad
Measured, 60 μrad

Figure 4

Figure 5

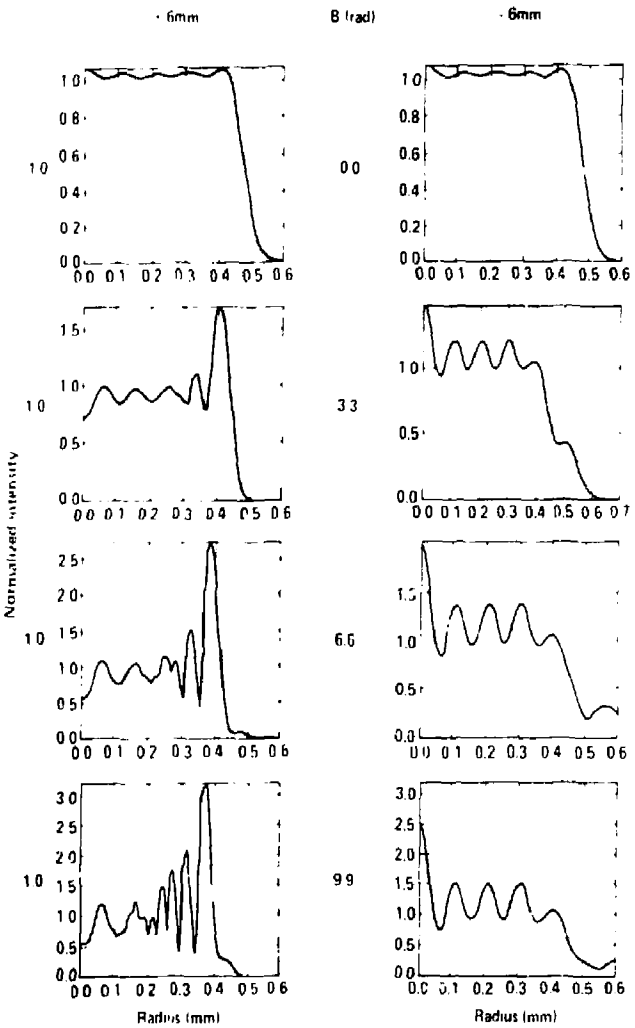
· 6mm
B (rad)
· 6mm
Normalized Intensity
1.0
0.0
3.3
6.6
9.9
Radius (mm)
Radius (mm)

Figure 6

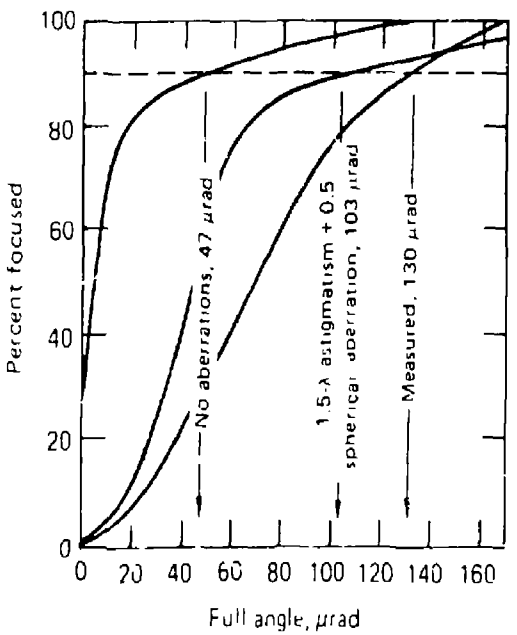
100
80
60
40
20
0
Percent focused
0
20
40
60
80
100
120
140
160
Full angle, μrad
No aberrations, 47 μrad
1.5-λ astigmatism + 0.5
spherical aberration, 103 μrad
Measured, 130 μrad

Figure 7